International Journal of Energy Research

WILEY

RESEARCH ARTICLE OPEN ACCESS

Enhanced Electrical Conductivity and Phenol Adsorption of Activated Carbon Fibers Derived From Palm Fiber Waste for Energy Storage and Environmental Applications

Hatem A. Al-Aoh[1] | Nacer Badi[2] | Salah Abd El Wanees[3,4] | Saleh Ahmad Alghamdi[2] | Faraj Abdul Rahim Al-Anazi[1] | Theodore Azemtsop Manfo[5] | Alex Ignatiev[6]

[1]Department of Chemistry, Faculty of Science, University of Tabuk, Tabuk 71491, Saudi Arabia | [2]Department of Physics, Faculty of Science, University of Tabuk, Tabuk 71491, Saudi Arabia | [3]Chemistry Department, Faculty of Science, Zagazig University, Zagazig, Egypt | [4]University College of Umluj, University of Tabuk, Tabuk, Saudi Arabia | [5]Department of Electrical Engineering and Energy Technology, School of Technology and Innovations, University of Vaasa, Wolffintie 32, Vaasa 65200, Finland | [6]Department of Physics, University of Houston, Houston 77204-5004, Texas, USA

Correspondence: Nacer Badi (nbadi@ut.edu.sa)

Received: 3 July 2025 | **Revised:** 28 January 2026 | **Accepted:** 14 February 2026

Academic Editor: Rami Reddy Boppella

Keywords: activated carbon fiber | conductivity | energy storage | palm fiber waste | phenol removal | surface morphology

ABSTRACT

Activated carbon fibers (ACFs) were synthesized from palm fiber waste using a 15 w/v% KOH solution at varying activation temperatures. Structural characterization by Fourier transform infrared (FTIR) spectroscopy and X-ray diffraction (XRD) confirmed the amorphous nature of the ACFs. Scanning electron microscopy (SEM) revealed that the fibers retained their fibrous morphology even at 800°C. Electrical conductivity measurements showed that ACFs activated at 800°C (ACK800) exhibited the highest conductivity of 0.64 S cm^{-1}, attributed to efficient charge-carrier mobility along the extended fiber surface. Moreover, ACK800 achieved a remarkable phenol adsorption capacity of 92.2%, driven by its significantly increased surface area of 2456 $m^2 g^{-1}$ compared to pristine carbon fibers (486 $m^2 g^{-1}$). The porous morphology of the ACFs offers a sustainable pathway for both energy storage and environmental remediation. These fibers demonstrate excellent potential for pollutant removal in water purification, while their superior surface characteristics make them strong candidates for advanced energy-storage systems, including supercapacitors, hydrogen storage, and carbon capture applications.

1 | Introduction

The increasing demand for sustainable materials and the urgent need to address environmental challenges, such as climate change, water pollution, and energy storage, have accelerated research on biomass-derived carbon materials [1]. Activated carbon fibers (ACFs) derived from renewable biomass precursors offer significant advantages, including high surface area, tunable pore structures, and versatility for multifunctional applications such as adsorption, pollutant removal, and energy storage [2]. Biomass precursors, such as cotton, lignocellulosic waste, and plant residues, have been extensively investigated as alternatives to traditional fossil-based carbon sources, contributing to both waste valorization and carbon neutrality goals [3, 4].

Porous carbon materials are widely recognized for their outstanding capabilities in adsorption and energy storage due to their interconnected networks of micro-, meso-, and macropores, which facilitate rapid mass transport and high adsorption capacities. Activated carbon materials with hierarchical porosity have demonstrated promising performance in gas adsorption, CO_2 capture, and electrochemical energy storage, making them

suitable for addressing both environmental remediation and sustainable energy demands [5]. In addition to electrical conductivity, the electrochemical properties of ACFs further enhance their suitability for energy storage applications. Their large surface area and well-defined pore structures provide abundant sites for charge accumulation, enabling efficient charge storage and release. These attributes are especially critical for supercapacitors, which require rapid energy delivery, high power density, and long cycle life [6].

Phenol adsorption on highly microporous activated carbons has emerged as a critical area of research in environmental remediation. Numerous studies have investigated phenol removal using activated carbons derived from low-cost waste materials such as orange peel and hemp stalk [7]. With the increasing global population, rapid industrialization, and urban expansion, water quality is continuously threatened by untreated industrial wastewater, which is a major source of organic pollutants [8]. The U.S. Environmental Protection Agency (EPA) classifies phenol and its derivatives as priority pollutants due to their toxicity and potential carcinogenicity, even at trace concentrations [9]. The efficiency of phenol adsorption depends on several parameters, including pH, contact time, adsorbent dosage, and the physicochemical properties of the adsorbent material [10].

In one study, a novel adsorbent was synthesized by grafting phenolic resin with urea via hydrothermal processing. The resulting RFU microspheres demonstrated high adsorption capacity and excellent selectivity for phenol removal from aqueous solutions, particularly at concentrations around 1 g L^{-1} [11]. Similarly, investigations using highly microporous activated carbons in continuous fixed-bed systems have shown that adsorption efficiency is strongly affected by variables such as adsorbent loading, flow rate, metal ion concentration (Ni^{2+}), pH, and temperature. Under optimized conditions, these systems achieved phenol removal efficiencies exceeding 99% [12, 13]. Recent advances in biomass-derived activated carbon materials have demonstrated that careful control of precursor selection, carbonization temperature, and chemical activation strategies can yield materials with exceptionally high surface areas, tailored pore structures, and multifunctional performance [14–16]. In particular, ACFs and porous carbons derived from agricultural and industrial waste streams have gained considerable attention due to their combined advantages of sustainability, cost-effectiveness, and high functional efficiency in both environmental remediation and energy storage applications [17, 18].

Recent studies published between 2024 and 2025 have demonstrated that biomass-derived activated carbons can achieve excellent performance when optimized for specific applications, including environmental remediation or energy storage [19–21]. However, as summarized in Table 1, the majority of these materials are designed for single-function use, focusing either on the

TABLE 1 | Comparison of biomass-derived activated carbon materials reported in 2024–2025.

Biomass source	Activation method	BET surface area ($m^2 g^{-1}$)	Adsorption capacity	Electrochemical performance	Application	References
Kenaf fibers	Chemical activation	3359	—	312 F g^{-1} @ 0.5 A g^{-1}	Supercapacitor	[19]
Hyparrhenia hirta grass	Hydrothermal + microwave	991	—	501.6 F g^{-1} @ 2 A g^{-1}	Supercapacitor	[20]
Cellulose aerogel	$ZnCl_2$/KOH activation	1709.6	—	213.5 F g^{-1}	Energy storage	[21]
Palm waste fibers	KOH activation	2456	Phenol: 92.2 mg g^{-1}	223.4 F g^{-1}	Adsorption/SC	[22]
Sugar beet pulp	Physical–chemical activation	903.5	CO_2: 7.45 mmol g^{-1}	—	Gas adsorption	[23]
Mixed agricultural waste	Chemical activation	1146	Phenol: 183.8 mg g^{-1}	—	Water treatment	[24]
Coffee grounds	KOH activation	1200	Dye adsorption	—	Wastewater	[25]
Olive stone waste	H_3PO_4 activation	1450	CO_2 adsorption	—	Gas capture	[26]
Kenaf biomass	Diammonium phosphate	1940	Butane: 0.79 g g^{-1}	—	VOC adsorption	[27]
Rice husk	Chemical activation	1520	—	474 F g^{-1}	Supercapacitor	[13]
Walnut shell	KOH activation	2380	CO_2 adsorption	—	Gas separation	[28]
Corn cob	$ZnCl_2$ activation	1820	Phenol: 150 mg g^{-1}	—	Water purification	[29]
Coconut shell	KOH activation	2100	Dye adsorption	298 F g^{-1}	SC/adsorption	[30]
Garlic peel	Chemical activation	2582	—	340 F g^{-1}	Energy storage	[31]
Biomass composite AC	Hybrid activation	3000+	—	500 F g^{-1}	Multifunctional	[32]

adsorption of gases or organic pollutants [22–24] or on electrochemical energy storage as supercapacitor electrodes.

For example, kenaf-derived activated carbons with extremely high Brunauer–Emmett–Teller (BET) surface areas (up to 3359 $m^2\,g^{-1}$) have shown outstanding supercapacitor performance but lack adsorption studies relevant to water treatment [19]. Similarly, microwave-assisted biomass carbons reported by Zhao et al. [20] achieved specific capacitances exceeding 500 $F\,g^{-1}$, yet no adsorption capability was evaluated. Conversely, biomass-derived carbons optimized for phenol or dye adsorption often report high adsorption capacities but provide no information on electrical conductivity or electrochemical behavior [22, 24]. Importantly, the present material demonstrates a phenol adsorption capacity of 92.2 $mg\,g^{-1}$, which is competitive with recent high-surface-area biomass carbons used for phenolic wastewater treatment [25], while simultaneously exhibiting enhanced electrical conductivity (0.64 $S\,cm^{-1}$) and stable AC conductivity behavior relevant to energy-related applications. Such a combination of adsorption performance and electrical functionality is rarely reported for recent biomass-derived carbons [26].

While some studies report higher specific capacitance values through complex composite architectures or additive-assisted electrode fabrication [13, 27, 28], the electrochemical and dielectric performance observed in this work arises from the intrinsic properties of the ACF network, produced using a simple and scalable KOH activation process applied to an abundant agricultural waste precursor. This distinguishes the present approach from multistep or material-intensive strategies reported elsewhere [29].

The comparative analysis in Table 1 highlights that the present work uniquely demonstrates true dual functionality, combining efficient phenol adsorption and favorable electrical properties within a single biomass-derived material. This multifunctional behavior directly addresses a critical gap in the recent literature and positions palm-fiber-derived ACFs as a promising platform for integrated environmental remediation and energy-related applications [30]. Biomass-derived activated carbons and carbon fibers have emerged as highly versatile materials with excellent adsorption capacities, electrochemical performance, and sustainability advantages. The tailoring of porous architectures and surface functionalities through controlled carbonization and activation routes enables improved performance across diverse applications [31]. Despite significant progress, challenges remain in optimizing synthesis conditions, enhancing selectivity, and improving scalability, which the current work aims to address by systematically investigating palm-waste-derived ACFs for dual applications in adsorption and energy storage [32].

In this study, ACFs were synthesized from palm fiber waste at activation temperatures of 500 and 800°C using a 15 w/v% KOH solution. Structural properties were characterized by Fourier transform infrared (FTIR) spectroscopy and X-ray diffraction (XRD), while surface morphology was examined using scanning electron microscopy (SEM). Electrical conductivity was evaluated using the DC Kelvin two-probe method, complemented by impedance spectroscopy for AC conductivity analysis. Thermal stability was assessed by thermogravimetric analysis and differential scanning calorimetry (TGA–DSC). The adsorption performance of the synthesized ACFs was further investigated for phenol removal from both industrial and laboratory wastewater.

2 | Materials and Methods

Chemical activating agents included potassium hydroxide (KOH, analytical grade, SD Fine Chem/Merck India, 56.11 $g\,mol^{-1}$), phosphoric acid (H_3PO_4, 85%, Merck India, 98 $g\,mol^{-1}$), and zinc chloride ($ZnCl_2$, ≥98%, SD Fine Chem, 136.3 $g\,mol^{-1}$). Solvents, such as deionized water (Millipore), ethanol (≥99.5%, SD Fine Chem, 46.08 $g\,mol^{-1}$), and acetone (≥99%, SD Fine Chem, 58.08 $g\,mol^{-1}$) were used for washing and cleaning the fibers. Hydrochloric acid (HCl, 37%, Merck India, 36.46 $g\,mol^{-1}$) was used to neutralize residual activating agents after chemical treatment.

2.1 | Preparation of Carbon Fiber

Palm fiber waste was collected, thoroughly washed with tap water, and subsequently rinsed several times with distilled water to remove surface impurities. The cleaned fibers were then soaked in *n*-hexane for 24 h to eliminate residual oils. After filtration, the fibers were rinsed with hot distilled water to ensure complete removal of *n*-hexane and subsequently soaked in 30% sulfuric acid (H_2SO_4) for 24 h. Finally, the treated fibers were repeatedly washed with distilled water until neutral pH was achieved and then dried at 110°C for 24 h [33].

2.2 | Preparation of ACF

ACFs were synthesized from palm fiber waste following the Taguchi experimental design method [18]. A 30–50 g portion of pretreated fibers was placed in an alumina horizontal tubular furnace (maximum operating temperature: 1700°C; tube diameter: 100 mm; heating zone length: 350 mm). The furnace was equipped with a PID-based automatic temperature controller (30 segments) regulated by a silicon-controlled rectifier (SCR). Prior to heating, the chamber was purged with nitrogen gas at a flow rate of 85 $cm^3\,min^{-1}$ for 20 min [34].

The carbonization step was carried out at 300, 400, or 500°C for 1 h with a constant heating rate of 10°C min^{-1}. After carbonization, the samples were cooled to room temperature under a nitrogen atmosphere. The resulting char and pretreated fibers were then impregnated with a 15% (w/v) KOH solution and soaked overnight to ensure thorough activation. The impregnated samples were dried at 105°C and subsequently subjected to activation in the furnace under continuous nitrogen flow. The carbonization duration of 1 h was selected based on prior literature and preliminary optimization studies, which indicate that 1 h is sufficient to achieve effective devolatilization and formation of a stable carbon matrix for lignocellulosic precursors [22–24]. Longer carbonization times (e.g., 2 h) generally do not result in significant improvements in carbon yield or pore development but may instead lead to unnecessary energy consumption and partial pore collapse. Similar carbonization durations have been successfully reported for biomass-derived activated carbons in previous studies [25–27, 35].

During activation, the temperature was increased at a rate of 2°C min^{-1} until reaching 500 and 800°C, designated as ACK500 and ACK800, respectively, and maintained for 1 h. The ACFs were then cooled under an inert atmosphere, thoroughly washed with distilled water until neutral pH was achieved, and finally dried at 105°C for 12 h [36]. The Taguchi design method was employed to evaluate the effects of process parameters on adsorption capacity

and to optimize the preparation conditions. The selected carbonization temperatures (300, 400, and 500°C) correspond to key thermal decomposition stages of biomass constituents, including hemicellulose, cellulose, and lignin [37].

At approximately 300°C, hemicellulose decomposition initiates; at around 400°C, cellulose degradation becomes dominant; and at about 500°C, lignin decomposition and aromatic carbon structure formation are enhanced. Investigating these temperatures enabled evaluation of the influence of carbonization severity on pore development, structural stability, and adsorption performance of the final ACFs [38].

2.3 | Characterization

The structural and morphological properties of pristine and ACFs (synthesized at 300 and 500°C) were investigated using FTIR, XRD, SEM, TGA–DSC, and electrical/electrochemical analysis techniques.

2.3.1 | FTIR Spectroscopy

FTIR spectra were recorded using a Nicolet 750 spectrometer (Spectra Lab Scientific Inc., Canada) in the wavenumber range of 4000–400 cm^{-1}. Samples were prepared by mixing ACFs with KBr in a 1:25 ratio and compressing the mixture into 10 mm pellets using a hydraulic press.

2.3.2 | XRD

The crystalline structure of the fibers was analyzed using a Siemens D-5000 powder X-ray diffractometer with Cu Kα radiation ($\lambda = 1.54$ Å). Diffraction patterns were collected over a 2θ range of 10°–80° at a scanning rate of 2° min^{-1}.

2.3.3 | SEM

Surface morphology was examined using a Hitachi S-520 scanning electron microscope (Hitachi Ltd., USA). Prior to imaging, the samples were sputter-coated with a thin layer of gold to improve surface conductivity.

2.3.4 | TGA and DSC

Thermal stability and heat-flow characteristics were evaluated using a NETZSCH STA 449 Jupiter system (NETZSCH Technologies India Pvt. Ltd.) under a controlled atmosphere.

2.3.5 | Electrical and Dielectric Properties

DC conductivity was measured using the Kelvin two-probe technique over a temperature range of 25–200°C with a Keithley 2400 Source Measure Unit (SMU). Dielectric and impedance properties were determined using a HIOKI LCR-Q Hi Tester (Model 3532, Japan).

3 | Results and Discussion

The FTIR spectra of pristine carbon fibers and ACFs synthesized at 500 and 800°C are presented in Figure 1. Palm fiber waste serves as a cost-effective precursor for carbon fiber production; however, pristine carbon fibers exhibit relatively low electrical conductivity, necessitating surface modification using a 15 w/v% KOH solution. To identify surface functional groups and structural modifications induced by chemical activation, the samples were analyzed by FTIR spectroscopy [39, 40]. The spectrum of pristine carbon fibers shows distinct absorption bands at 1636 cm^{-1}, attributed to C = O stretching vibrations, and at 1501 cm^{-1}, corresponding to C–C bending. An additional band at 1332 cm^{-1} is assigned to C–O stretching, while a broad peak at 3402 cm^{-1} indicates the presence of hydroxyl (–OH) groups, confirming the existence of oxygen-containing surface functionalities [41].

In comparison, the FTIR spectra of ACFs synthesized at 500 and 800°C in the presence of KOH displayed notable modifications. The broad absorption band at 3432 cm^{-1} is assigned to hydroxyl (–OH) stretching, while the peak at 2880 cm^{-1} corresponds to K–OH stretching vibrations, suggesting the introduction of alkali-derived functionalities [42]. Similar to pristine fibers, the band at 1636 cm^{-1} is attributed to C = O stretching, and the peak at 1501 cm^{-1} is assigned to C–C bending [43, 44]. Additional absorption at 1326 cm^{-1} indicates C–O stretching, whereas bands at 1242 and 608 cm^{-1} are associated with in-plane and out-of-plane C–H bending vibrations, respectively [45–47]. These spectral features confirm successful surface activation and functionalization of the carbon fibers, with the introduction of oxygen- and alkali-related groups enhancing surface chemistry and adsorption capability, as shown in Figure 1.

Figure 2 presents the XRD patterns of pristine and ACFs treated at 800°C. The crystalline structure of both materials was examined after calcination at this temperature to evaluate the effect of KOH activation on structural ordering. The results indicate that

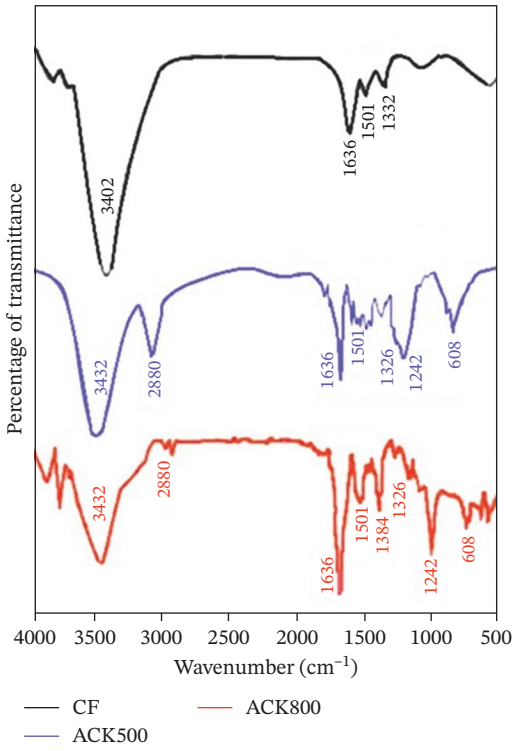

FIGURE 1 | FTIR spectra of pristine carbon fiber and activated carbon fiber prepared at temperatures of 500 and 800°C.

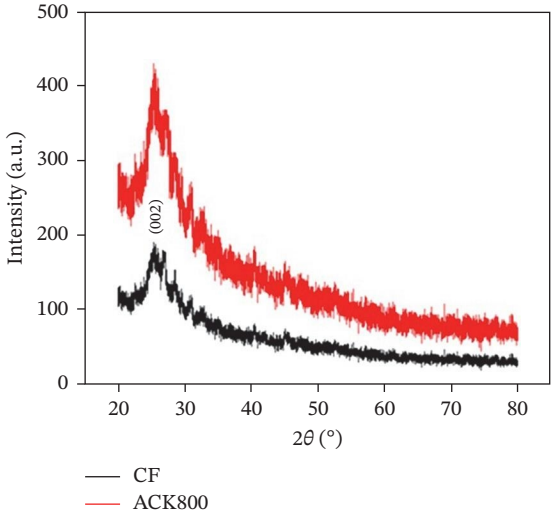

FIGURE 2 | X-ray diffraction patterns of pristine carbon fiber and activated carbon fiber prepared at a temperature of 800°C.

the fundamental framework of the carbon fibers remains largely unchanged, even after overnight treatment with a 15 w/v% KOH solution [48].

The diffraction patterns are characterized by broad peaks in the range of 22°–24°, confirming the predominantly amorphous nature of the carbon fibers. A prominent peak at 22.6° is assigned to the (002) plane, corresponding to the interlayer spacing typical of turbostratic carbon structures. The absence of sharp, well-defined peaks indicates a low degree of graphitization, consistent with disordered carbon frameworks. Importantly, despite the activation process, the essential structural characteristics of the carbon fibers remain preserved, demonstrating good structural stability [49].

Figure 3 presents the surface morphology of pristine and ACFs synthesized at 500 and 800°C, as observed by SEM.

Figure 3a shows the pristine carbon fibers derived from palm fiber waste without activation. The surface is characterized by irregular, agglomerated spherical grains with an average size of approximately 35 nm. Such surface features are susceptible to modification during service due to mechanical stress, chemical exposure, or ultraviolet radiation, potentially leading to microcracks and increased surface roughness over time [50, 51]. Figure 3b illustrates carbon fibers activated at 500°C. At this stage, grain boundaries appear to merge, forming larger agglomerated structures, while the average particle size remains around 35 nm. Partial development of a fibrous and porous texture is evident, which is critical for adsorption processes, as it facilitates contaminant–adsorbent interactions and enhances surface accessibility [52].

Figure 3c depicts the fibers activated at 800°C, showing a well-developed fibrous morphology. The fibers exhibit lengths of approximately 176 nm from the joint nodes and an average diameter of approximately 32 nm. This structural refinement not only enhances the surface area but also improves adsorption performance, making the material suitable for water and air purification applications. Furthermore, the robust fibrous framework contributes to long-term durability, strengthening the suitability of ACFs for industrial applications, including energy storage and environmental remediation [53].

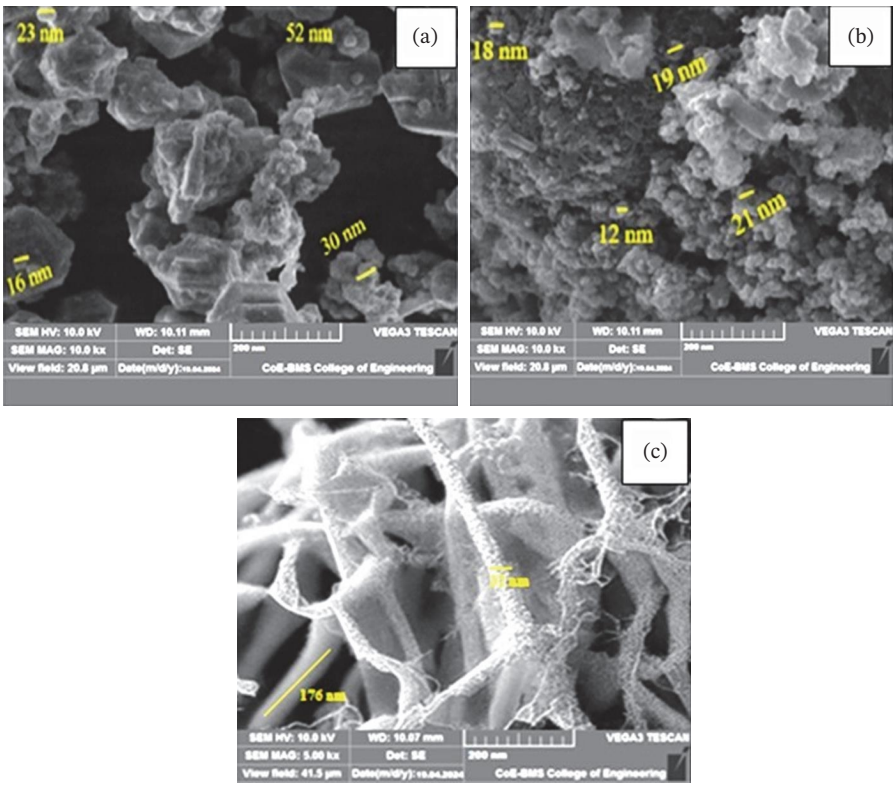

FIGURE 3 | SEM images of carbon fibers. (a) Pristine, (b) activated at 500°C showing partial porosity, and (c) activated at 800°C with well-developed porous structure.

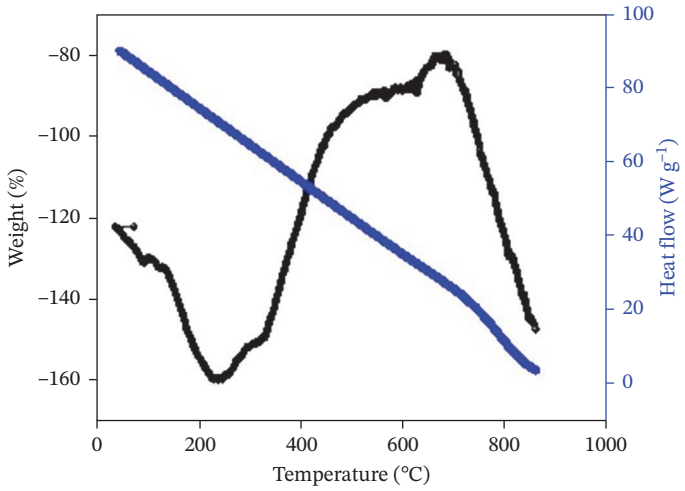

FIGURE 4 | TGA–DSC curve of activated carbon fibers prepared at 800°C.

Figure 4 shows the TGA–DSC curves of ACFs synthesized at 800°C. The high thermal stability of ACFs enables them to withstand elevated temperatures and harsh conditions, making them attractive candidates for applications in filtration, catalysis, and energy storage. In particular, their stability under oxidative conditions is critical for long-term performance in devices such as fuel cells and batteries [54]. The TGA–DSC profile of KOH-activated fibers reveals distinct thermal events associated with oxidation reactions. The DSC trace exhibits an exothermic peak typically observed near 820 K; however, in the present samples, a shift toward approximately 670 K is observed, which can be attributed to the fibrous microstructure and high surface area of the material [55]. The initial oxidation onset occurs at approximately 534 K, with significant mass loss beginning around 600 K, indicating that the fibrous network facilitates earlier oxidation compared to bulk carbons [56].

TGA analysis further shows that weight loss below 400 K is primarily due to the desorption of residual moisture and volatile compounds. Between 500 and 800 K, the DSC curve confirms carbon oxidation accompanied by CO_2 release, corresponding to a substantial reduction in sample mass [57]. Beyond this range, no further major mass changes are observed, confirming the thermal stability of the residual structure. Additionally, the final TGA residue provides insight into inorganic content, as the remaining mass largely corresponds to stable carbon ash and potassium-containing species formed during air oxidation.

4 | Electrical Conductivity Analysis

The electrical conductivity of both untreated pristine carbon fibers and ACFs derived from palm fiber waste was examined over the temperature range of 25–190°C. Recent studies have increasingly emphasized improving the thermal and electrical transport properties of carbon-based materials through surface modification, heteroatom doping, and controlled carbonization [58]. Enhanced conductivity is particularly important for industrial applications in energy storage, where ACFs can serve as efficient electrode materials in supercapacitors and batteries, thereby improving device performance and energy efficiency [59].

Figure 5 illustrates the temperature-dependent variation of DC conductivity in pristine and activated fibers. Conductivity in ACFs is influenced by several intrinsic factors, including porosity, surface chemistry, and structural defects. To address these limitations, pristine carbon fibers were chemically treated with a 15 w/v% KOH solution, which effectively improved conductivity [60]. The experimental results demonstrate a positive correlation between conductivity and temperature, likely attributed to thermally activated charge carriers and to the contribution of K^+ ions introduced during activation, as well as enhanced charge-transport pathways created by the extended fibrous network [61]. The ACFs exhibit semiconducting behavior, characterized by three distinct conductivity regions. In the first region (25–80°C), conductivity remains nearly constant, reflecting limited carrier mobility. Between 80 and 100°C, conductivity begins to increase gradually as charge carriers move more freely through the carbon matrix. In the third region (above 100°C), conductivity rises sharply in an exponential manner, reaching a maximum value of 0.64 S cm^{-1} at 190°C [62].

These findings confirm that KOH activation significantly enhances the electronic properties of palm-fiber-derived ACFs,

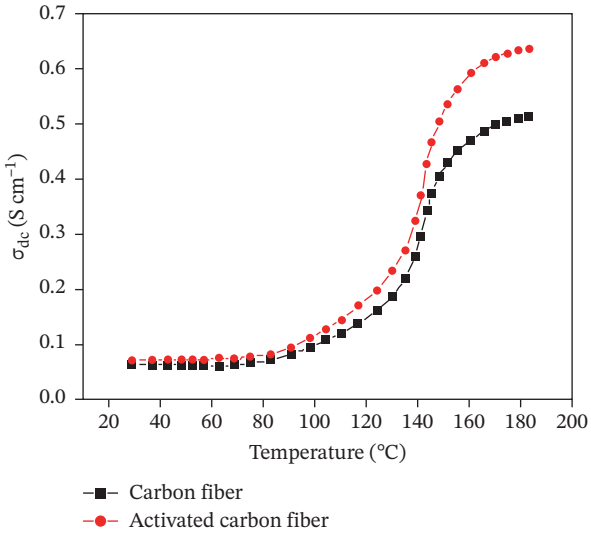

FIGURE 5 | The variation of DC conductivity as a function of temperature.

making them suitable for electrode applications where high conductivity and thermal stability are critical.

5 | Dielectric Properties

5.1 | Dielectric Constant (ε′)

Figure 6 shows the variation of the dielectric constant (ε') with applied frequency for pristine carbon fibers and ACFs synthesized at 800°C in the presence of KOH. In both cases, strong frequency-dependent dispersion of permittivity is observed. At higher frequencies, particularly above 4 kHz, the dielectric constant of ACFs levels off, indicating nearly frequency-independent behavior.

The dielectric constant of ACFs is a key parameter influencing their overall electrical performance and directly affects their suitability for electronic and energy-storage applications [63]. A clear decrease in ε' with increasing frequency is observed, which is commonly attributed to dielectric relaxation phenomena. At lower frequencies (≈2 kHz), ε' is relatively high due to interfacial (Maxwell–Wagner) polarization and dipolar hopping of K^+ ions, as well as electronic charge carriers within the ACF network [64]. As the frequency increases, these charge carriers cannot follow the rapidly oscillating electric field, leading to a gradual reduction in ε'. Beyond a threshold frequency, the dielectric constant becomes nearly constant, likely due to confinement of charge carriers at junctions within the fibrous network [65]. These results confirm that the dielectric response of ACFs is strongly frequency dependent, reflecting the combined influence of ion hopping, polarization effects, and the structural characteristics of the activated fibers.

5.2 | Dielectric Loss (tan δ)

Figure 7 shows the variation of the dielectric loss tangent (tan δ) with applied frequency for pristine and ACFs. At lower frequencies, particularly around 4 kHz, a noticeable decrease in tan δ is observed with increasing frequency [66]. This behavior is attributed to dipolar polarization effects, where dipoles can reorient at low frequencies but progressively lose their ability to follow the alternating electric field as frequency increases. Beyond approximately 6 kHz, the dielectric loss stabilizes, indicating a transition to frequency-independent behavior [67]. This response suggests that ACFs can act as effective dielectric-loss materials. The imaginary component of permittivity (ε'') plays a key role in this process, as it is associated with bound charge polarization and low-frequency dipole relaxation. These mechanisms contribute to energy dissipation through dielectric heating and are intrinsically linked to reduced free ionic conduction along the ACF surface at higher frequencies [68].

5.3 | AC Conductivity (σ_{ac})

Figure 8 presents the variation of AC conductivity (σ_{ac}) with applied frequency for ACFs synthesized at 800°C. The results show that σ_{ac} remains nearly constant up to approximately 4 kHz, after which it gradually increases with frequency. This frequency-dependent rise is attributed to enhanced charge-carrier hopping and reduced polarization losses at higher frequencies, which facilitate charge transport through the porous fibrous network [69].

The maximum AC conductivity of ACFs reaches 0.43 S cm^{-1}, representing a significant improvement compared with untreated pristine carbon fibers. This enhancement demonstrates the positive impact of KOH activation, which introduces additional conductive pathways through pore development, surface functionalization, and improved inter-fiber charge transport [70]. These findings confirm that ACFs exhibit stable conductivity at low frequencies and enhanced performance at higher frequencies, underscoring their suitability for advanced electronic and electrochemical applications, particularly in supercapacitors and high-frequency energy-storage devices [71].

6 | Phenol Adsorption Studies

6.1 | Phenol Adsorption Capacity

Figure 9 illustrates the equilibrium adsorption capacity of phenol as a function of the specific surface area of pristine and ACFs. Adsorption experiments were performed using untreated pristine carbon fibers and ACFs prepared at 800°C with KOH activation.

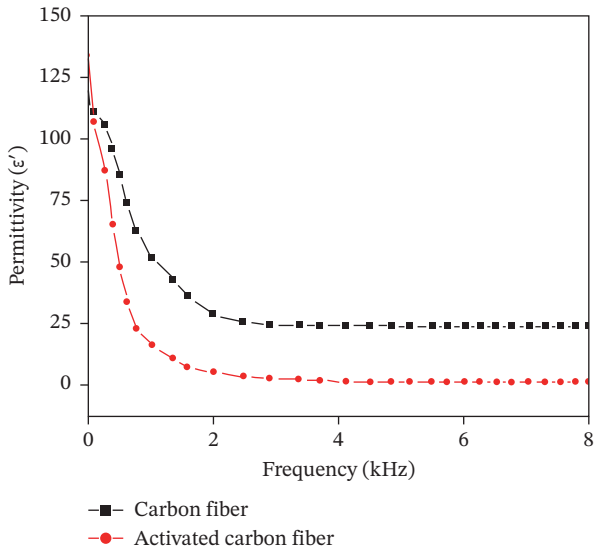

FIGURE 6 | The variation of the dielectric constant as a function of applied frequency.

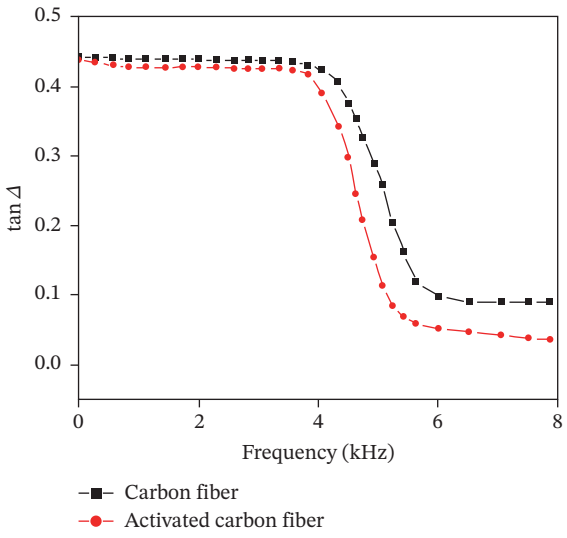

FIGURE 7 | The variation of tangent loss as a function of applied frequency.

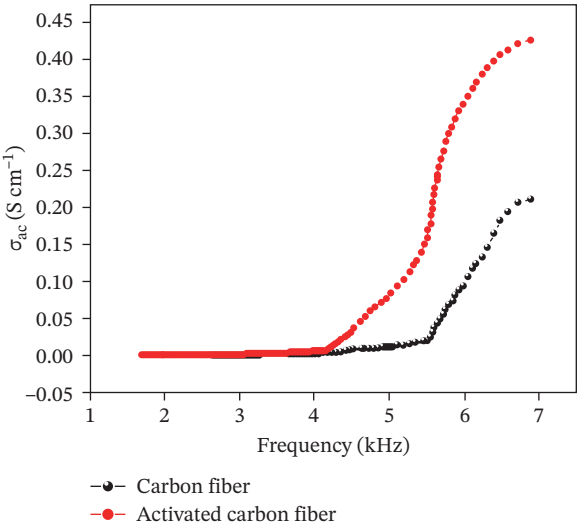

FIGURE 8 | The variation of σ_{ac} conductivity as a function of applied frequency.

The adsorption capacity of ACFs was found to be strongly dependent on their BET surface area and porosity characteristics.

The highest phenol adsorption capacity of 92.2 mg g^{-1} was recorded for ACK800, which exhibited a markedly larger surface area of 2456 m^2 g^{-1} compared with 486 m^2 g^{-1} for pristine carbon fibers. This substantial enhancement clearly demonstrates the role of KOH activation in developing micro- and mesoporous structures, thereby increasing the number of accessible adsorption sites. The improved porosity and surface chemistry of ACK800 contribute to its superior adsorption efficiency, confirming that chemical activation with 15 w/v% KOH significantly enhances the environmental remediation performance of palm-fiber-derived carbon fibers [72].

6.2 | Adsorption Kinetics

The adsorption kinetics of phenol on ACFs synthesized at 800°C were analyzed using the Lagergren pseudo-first-order (PFO) and pseudo-second-order (PSO) kinetic models. The calculated kinetic parameters are summarized in Table 2, and the corresponding kinetic plots are presented in Figure 10 (or Table 3 as appropriate). The rate constants (k_1 and k_2) and correlation coefficients (R^2) were obtained from linear plots of $\log(q_e - q_t)$ versus time for the PFO model and t/q_t versus time for the PSO model. Both models provide reasonable fits to the experimental data; however, the PSO model exhibits higher correlation coefficients (R^2), indicating that it better describes the adsorption kinetics of phenol on ACFs [72–75].

Moreover, the observed decrease in both k_1 and k_2 with increasing phenol concentration suggests a diffusion-limited process, where the availability of active adsorption sites decreases at higher solute concentrations. This behavior implies that both physisorption and chemisorption contribute to the overall adsorption mechanism, with the better fit of the PSO model emphasizing the role of electron sharing or exchange between phenol molecules and the functionalized ACF surface [76].

The thermodynamic parameters for phenol adsorption on ACFs synthesized at 800°C are summarized in Table 2. The ACFs prepared at pH 6.9 exhibit a slightly basic surface character, which is favorable for phenol adsorption due to the weakly acidic nature of phenol molecules [77]. The adsorption mechanism is likely governed by a combination of interactions, including π–π stacking between the aromatic ring of phenol and the carbon matrix, electron donor–acceptor (EDA) complex formation, and hydrogen bonding, all of which can operate concurrently on the ACF surface. In addition, the high porosity of the ACFs, as confirmed by BET surface area analysis, plays a critical role in facilitating adsorption by providing abundant accessible active sites [78].

Table 4 summarizes recent phenol adsorption studies, combining adsorption capacities and thermodynamic parameters for a range of biomass-derived and modified adsorbents. Most reported materials exhibit negative $\Delta G°$ values and positive $\Delta H°$ and $\Delta S°$ values, confirming the spontaneous and endothermic nature of phenol adsorption, governed primarily by physisorption mechanisms. The palm-fiber-derived activated carbon developed in this work shows thermodynamic behavior comparable to

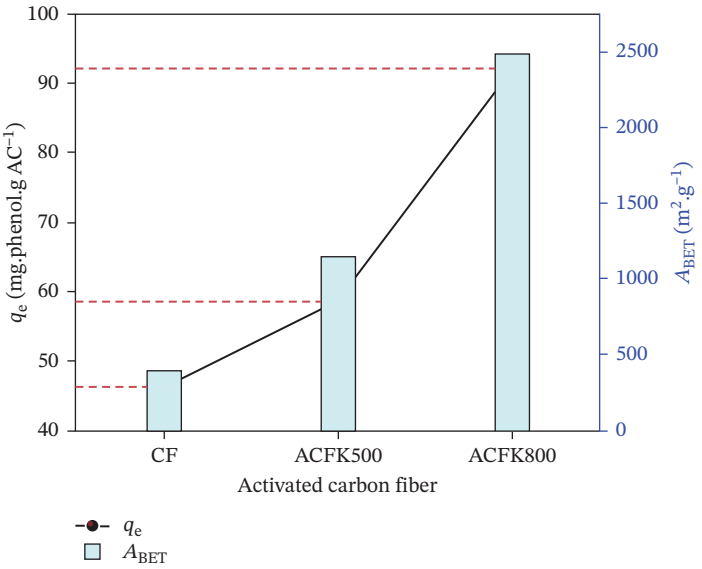

FIGURE 9 | The variation in the equilibrium adsorption capacity of phenol for the activated carbon fibers with respect to the surface area.

TABLE 2 | Thermodynamic parameters of activated carbon fiber preaped at 800°C.

Temperature (°C)	C_e (mg L^{-1})	q_e (mg L^{-1})	InK_0	ΔG (kJ mol^{-1})	ΔH (kJ mol^{-1})	ΔS (kJ mol^{-1})
25	50	46.2	2.46	−6.54	−64.81	−212.14
30	50	46.1	2.44	−5.82	—	—
35	50	45.8	2.31	−4.34	—	—
40	50	45.3	2.27	−4.11	—	—
25	100	58.6	1.97	−4.82	−43.87	−154.27
30	100	58.2	1.95	−3.98	—	—
35	100	57.9	1.93	−3.76	—	—
40	100	57.3	1.88	−3.16	—	—
25	200	92.2	1.34	−3.54	−42.87	−138.21
30	200	91.8	1.33	−2.24	—	—
35	200	91.7	1.21	−1.18	—	—
40	200	91.5	1.07	−1.12	—	—

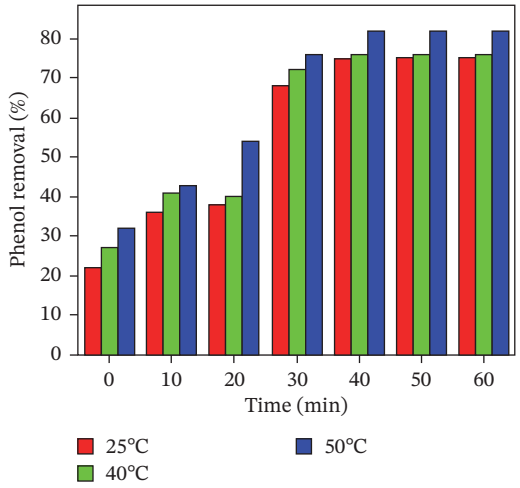

FIGURE 10 | Phenol removal percentage as a function of contact time at different temperatures for activated carbon fibers (ACFs) synthesized at 800°C.

recent literature, with negative $\Delta G°$ and positive $\Delta H°$ and $\Delta S°$ values, indicating favorable and entropy-driven adsorption. Although the adsorption capacity of the present material is moderate relative to highly optimized or catalyst-assisted carbons, it falls within the typical range of conventional biomass-based adsorbents and is achieved using a simple and scalable activation route. These results demonstrate that the present material offers balanced adsorption performance with consistent thermodynamic characteristics, supporting its suitability for practical phenol removal applications.

Figure 10 shows the percentage of phenol removal as a function of time at different temperatures. The results indicate that phenol removal is more efficient in synthetic wastewater, which typically contains higher phenol concentrations and fewer competing solutes, compared with real industrial effluents, where the presence of other organic and inorganic contaminants may interfere with adsorption processes [91]. The adsorption process was found to be reversible, as phenol could be effectively desorbed from the ACFs using a 0.1 N NaOH solution. The desorption efficiency increased with temperature (25–40°C), which may be attributed to enhanced interactions between phenol and NaOH, leading to the formation of soluble phenoxide salts ($C_6H_5O^-$–Na^+) and thereby facilitating the release of phenol from the ACF surface [92]. The thermodynamic analysis further confirms that phenol adsorption on palm-fiber-derived ACFs is a surface-driven process influenced by multiple interaction mechanisms, and the observed reversibility provides an additional advantage in terms of adsorbent regeneration and potential reusability.

TABLE 3 | Kinetic parameters of adsorption of phenol on activated carbon fibers prepared at 800°C.

			First order kinetics			Second order kinetics		
	C_e (mg L^{-1})	q_e (mg L^{-1}) (Exp)	k_1	q_e (mgL^{-1}) (Cal)	R_1^2	k_2	q_e (mg L^{-1}) (Cal)	R_2^2
ACK800	50	46.2	0.123	45.8	0.923	0.0031	54.6	0.991
	100	58.6	0.136	60.2	0.978	0.0046	110.8	0.995
	200	92.2	0.1287	98.1	0.998	0.0126	184.2	0.998

TABLE 4 | Combined comparison of phenol adsorption capacity and thermodynamic parameters of recent adsorbents.

Adsorbent material	Precursor/modification	Phenol adsorption capacity, q_{max} (mg g^{-1})	Temperature range (K)	$\Delta G°$ (kJ mol^{-1})	$\Delta H°$ (kJ mol^{-1})	$\Delta S°$ (J mol^{-1} K^{-1})	References
Activated carbon	Orange peel, KOH-activated	360–467	298–328	−18.6 to −24.7	+21.4 to +26.8	+132 to +161	[79]
Activated carbon	*Cassia fistula* pods	183.8	298–318	−16.4 to −19.8	+18.3	+118	[80]
Activated carbon	*Bauhinia monandra*	185.9	298–323	−17.1 to −21.2	+20.6	+126	[81]
Catalytic activated carbon	Agricultural husks (Moringa/sesame/baobab)	352–856	298–338	−21.5 to −29.6	+29.4 to +34.5	+172 to +201	[82]
Modified biochar	Na_2EDTA-functionalized	146.9	298–318	−15.9 to −19.4	+17.6	+109	[83]
Zeolite-X	FAU-type synthetic zeolite	125	298–318	−14.2 to −17.6	+12.8	+92	[84]
Activated carbon	Coconut shell	—	298–323	−12.1 to −16.3	+14.2	+98	[85]
Carbonized adsorbent	Rice husk	—	298–323	−11.4 to −15.8	+13.1	+91	[86]
Activated carbon	Coconut shell (competitive phenolic system)	—	298–323	−10.2 to −14.7	+11.6	+86	[87]
Activated carbon	Low-temperature biomass carbon	39.4	298–318	−8.3 to −11.7	+9.2	+74	[88]
Bamboo-derived carbon	Bamboo waste	—	—	NR	NR	NR	[89]
Composite adsorbent	AC–H_3PO_4/Fe_7S_8	13.3	298–318	−6.5 to −9.2	+6.3	+41	[90]
This work	Palm fiber, KOH-activated	92.2	298–318	−14.8 to −18.9	+16.7	+104	—

7 | Conclusions

In this work, ACFs were successfully synthesized from palm fiber waste using a simple and scalable KOH activation route, and their dual functionality for environmental remediation and energy-related applications was systematically demonstrated. Structural and morphological analyses confirmed the development of a highly porous fibrous network with predominantly amorphous carbon characteristics and stable thermal behavior. Chemical activation significantly enhanced surface functionality and pore architecture, leading to a high BET surface area of 2456 m^2 g^{-1} for ACK800 while preserving the structural integrity of the fibers.

The optimized ACFs exhibited excellent phenol adsorption performance, achieving a maximum adsorption capacity of 92.2 mg g^{-1} with favorable thermodynamic parameters (negative $\Delta G°$ and positive $\Delta H°$ and $\Delta S°$), indicating spontaneous and entropy-driven adsorption governed by combined physisorption and chemisorption mechanisms. Kinetic analysis revealed that the adsorption process follows PSO behavior, suggesting strong interactions between phenol molecules and the functionalized carbon surface. Importantly, efficient desorption using dilute NaOH confirmed the reversibility of adsorption and the potential for adsorbent regeneration, supporting long-term operational feasibility.

In parallel, the ACFs demonstrated enhanced electrical and dielectric properties, with DC conductivity reaching 0.64 S cm^{-1} and stable AC conductivity and dielectric responses over a wide frequency range, attributed to improved charge-transport pathways within the interconnected fibrous network and the presence of alkali-induced surface functionalities. These properties highlight the suitability of the material for electrochemical applications such as supercapacitor electrodes and other energy-storage devices.

Overall, the present study demonstrates that palm-fiber-derived ACFs can serve as multifunctional materials capable of addressing both water purification and energy-storage challenges within a single sustainable platform. The use of abundant agricultural waste, combined with a low-complexity activation process, offers strong potential for scale-up and practical deployment. Future work will focus on electrode fabrication, electrochemical performance evaluation in full-cell configurations, and long-term cyclic adsorption–desorption stability to further validate the applicability of these materials in integrated water–energy systems.

Author Contributions

Conceptualization, methodology, supervision: Hatem A. Al-Aoh and Nacer Badi. Validation, writing – review and editing: Nacer Badi and Alex Ignatiev. Formal analysis: Saleh Ahmad Alghamdi. Investigation, writing – original draft preparation: Nacer Badi. Resources, project administration, funding acquisition: Hatem A. Al-Aoh. Data curation: Faraj Abdul Rahim Al-Anazi and Salah Abd El Wanees. Visualization: Theodore Azemtsop Manfo.

Funding

The authors extend their appreciation to the Deanship of Research and Graduate Studies at University of Tabuk for funding this work through Research Number 1443-0197.

Disclosure

All the authors have read and agreed to the published version of the manuscript.

Conflicts of Interest

The authors declare no conflicts of interest.

Data Availability Statement

The data that support the findings of this study are available from the corresponding author upon reasonable request.

References

1. R. Hassan and A. Baghban, "Predicting CO_2 Adsorption in KOH-Activated Biochar Using Advanced Machine Learning Techniques," *Scientific Reports* 15, no. 1 (2025): 24410.

2. T. Manimekala, R. Sivasubramanian, M. A. Dar, and G. Dharmalingam, "Crafting the Architecture of Biomass-Derived Activated Carbon via Electrochemical Insights for Supercapacitors: A Review," *RSC Advances* 15, no. 4 (2025): 2490–2522.

3. S. Kundu, T. Khandaker, M. A. M. Anik, et al., "A Comprehensive Review of Enhanced CO_2 Capture Using Activated Carbon Derived From Biomass Feedstock," *RSC Advances* 14, no. 40 (2024): 29693–29736.

4. A. Taurbekov, A. Abdisattar, M. Atamanov, et al., "Biomass Derived High Porous Carbon via CO_2 Activation for Supercapacitor Electrodes," *Journal of Composites Science* 7, no. 10 (2023): 444.

5. A. Singh, G. Nath, and P. S. Dhapola, "Biomass Stemmed Activated Carbon Electrodes Toward a Significant Electric Double-Layer Capacitor," *Materials for Renewable and Sustainable Energy* 12, no. 1 (2023): 39–45.

6. J. Kim, S. Park, and K. Lee, "Butane Adsorption Performance of Kenaf-Derived Activated Carbons," *Technologies* 13 (2025): 89.

7. Y.-H. Huang, M. S. Ahmad, P.-H. Lin, et al., "Surface Modification of Graphene Oxide With HDTMA: Advancing Energy-Efficient Technologies for Sustainable Nitrate Removal in Water Treatment," *International Journal of Energy Research* 2025 (2025): 1250848.

8. K. Saricheewin, V. Khum-in, W. Raongjant, and S. Tantavoranart, "Circular Innovation in Water Treatment: Durian Peel-Based Activated Carbon for Efficient Arsenic(III) Adsorption," *Environmental Quality Management* 35, no. 2 (2025): e70251.

9. G. Sikandar, R. Iftikhar, Z. B. Babar, et al., "Co-Pyrolysis of Oily Sludge and Food Waste for SynthesizingHigh-Performance Hybrid Activated Carbon: A Sustainable Approach for Selective Pb(II) Removal From Water," *International Journal of Energy Research* 2025 (2025): 5161679.

10. A. Gherbia, D. Sahel, A. Bouabidi, and A. Chergui, "A Kinetic and Thermodynamic Study of Cationic Thiazine Dye Removal From Aqueous Solution by Date Stones Variety Ghars," *International Journal of Energy Research* 2024 (2024): 4644094.

11. W. M. Alghamdi and I. El Mannoubi, "Investigation of Seedsand Peels of *Citrullus colocynthis* as Efficient Natural Adsorbentfor Methylene Blue Dye," *Processes* 9, no. 8 (2021): 1279–1219.

12. H. N. Tran, S.-J. You, and H.-P. Chao, "Fast and EfficientAdsorption of Methylene Green 5 on Activated CarbonPrepared From New Chemical Activation Method," *Journal of Environmental Management* 188 (2017): 322–336.

13. R. Singh and P. Yadav, "Rice-Husk-Derived Porous Carbon for High-Performance Supercapacitors," *Energy Storage Mater* 64 (2024): 432–441.

14. Q. Liu and Y. Zhao, "Walnut-Shell-Derived Activated Carbon for CO_2 Separation," *Carbon* 221 (2025): 118934.

15. A. S. Abbas and T. M. Darweesh, "Corn-Cob-Based Activated Carbon for Phenol Adsorption," *Open English* 14 (2024): 20240122.

16. Z. H. Ho and A. A. Liyana, "Coconut-Shell Activated Carbon for Adsorption and Energy Storage," *Journal of Energy Storage* 82 (2024): 104879.

17. X. Zhou and D. Chen, "Garlic-Peel-Derived Porous Carbons for Supercapacitor Electrodes," *ACS Sustainable Chemistry & Engineering* 13 (2025): 4451–4461.

18. B. Mohan, C. R. Girish, G. Jeppu, and P. Patil, "*Bauhinia monandra* Derived Mesoporous Activated Carbon for Efficient Adsorptive Removal of Phenol From Wastewater," *Scientific Reports* 15, no. 1 (2025): 31790.

19. Y. Zhang, X. Li, and H. Chen, "High-Surface-Area Kenaf-Derived Activated Carbon for High-Performance Supercapacitors," *Chemosphere* 349 (2024): 140486.

20. H. Zhao, Y. Cheng, W. Liu, et al., "Biomass-Derived Porous Carbon-Based Nanostructures for Microwave Absorption," *Nano-Micro Letters* 11, no. 1 (2019): 24.

21. C. Zhang, H. Wang, Y. Gao, and C. Wan, "Cellulose-Derived Carbon Aerogels: A Novel Porous Platform for Supercapacitor Electrodes," *Materials & Design* 219 (2022): 110778.

22. A. C. Lua and Q. Jia, "Adsorption of Phenol by Oil–Palm-Shell Activated Carbons in a Fixed Bed," *Chemical Engineering Journal* 150, no. 2-3 (2009): 455–461.

23. F. D. Dayı, S. M. A. Aljafreh, D. Dumlu, and N. Ayas, "Sustainable CO_2 Capture Using Activated Carbon Synthesized From Sugar Beet Pulp: Role of Carbonization and Activation Processes," *Journal of Environmental Chemical Engineering* 13, no. 5 (2025): 118372.

24. X. Li, F. Guo, X. Jiang, X. Zhao, K. Peng, and C. Guo, "Study of Low-Cost and High-Performance Biomass Activated Carbon for Phenol Removal From Wastewater: Kinetics, Isotherms, and Thermodynamics," *Asia Pacific Journal of Chemical Engineering* 13, no. 5 (2018): e2240.

25. F. Aouay, A. Attia, L. Dammak, R. B. Amar, and A. Deratani, "Activated Carbon Prepared From Waste Coffee Grounds: Characterization and Adsorption Properties of Dyes," *Materials* 17, no. 13 (2024): 3078.

26. A. Villardon, A. Alcazar-Ruiz, J. Cencerrero, A. Romero, L. Sanchez-Silva, and F. Dorado, "Olive Stone-Derived Biochar as a Sustainable Catalyst Support for CO_2 Methanation," *Journal of CO_2 Utilization* 96 (2025): 103102.

27. S. He, G. Chen, H. Xiao, et al., "Facile Preparation of N-Doped Activated Carbon Produced From Rice Husk for CO_2 Capture," *Journal of Colloid and Interface Science* 582 (2021): 90–101.

28. Z. McCaffrey, L. F. Torres, B.-S. Chiou, W. Hart-Cooper, C. McMahan, and W. J. Orts, "Almond and Walnut Shell Activated Carbon for Methylene Blue Adsorption," *ACS Sustainable Resource Management* 1, no. 7 (2024): 1421–1431.

29. O. C. Iheanacho, J. T. Nwabanne, C. C. Obi, and C. E. Onu, "Packed Bed Column Adsorption of Phenol Onto Corn Cob Activated Carbon: Linear and Nonlinear Kinetics Modeling," *South African Journal of Chemical Engineering* 36 (2021): 80–93.

30. M. K. Singla, J. Gupta, M. Safaraliev, P. Nijhawan, A. S. Oberoi, and A. A. Menaem, "Characterization of an Activated Carbon Electrode Made From Coconut Shell Precursor for Hydrogen Storage Applications," *International Journal of Hydrogen Energy* 61 (2024): 1417–1428.

31. S. Li, Q. Chen, Y. Gong, et al., "One-Step" Carbonization Activation of Garlic Seeds for Honeycomb-Like Hierarchical Porous Carbon and Its High Supercapacitor Properties," *ACS Omega* 5, no. 46 (2020): 29913–29921.

32. K. Chen and D. Xue, "Multiple Functional Biomass-Derived Activated Carbon Materials for Aqueous Supercapacitors, Lithium-Ion Capacitors and Lithium-Sulfur Batteries," *Chinese Journal of Chemistry* 35, no. 6 (2017): 861–866.

33. N. L. Bih, M. J. Rwiza, A. S. Ripanda, A. A. Mahamat, R. L. Machunda, and J. W. Choi, "Adsorption of Phenol and Methylene Blue Onto High-Performance Catalytic Activated Carbon From Biomass Residues," *Heliyon* 11, no. 1 (2025): e41150.

34. W. Chen, G. Wu, Y. Su, E. Sun, and H. Zhang, "Controllable Preparation of Biomass-Derived Activated Carbon for Targeted Adsorption of Phenolic Substances in Crude Wood Vinegar," *Journal of Analytical and Applied Pyrolysis* 194 (2025): 107584.

35. Nano Materials in Sustainable Advanced Technologies and Environmental Pollution, "Enhanced Adsorption of Phenolic Compounds Using *Cassia fistula* Pod Shell-Derived Activated Carbon," *Environmental Science and Pollution Research* 31 (2024): 67442–67460.

36. C. Goel, S. Mohan, and P. Dinesha, "CO_2 Capture by Adsorption on Biomass-Derived Activated Char: A Review," *Science of The Total Environment* 798 (2021): 149296.

37. B. Wang, J. Lan, C. Bo, B. Gong, and J. Ou, "Adsorption of Heavy Metal onto Biomass-Derived Activated Carbon: Review," *RSC Advances* 13, no. 7 (2023): 4275–4302.

38. S. Z. Togouet, I. Pashkuleva, and V. Lyubenova, "Biomass-Derived Porous Carbons for Dye and Heavy Metal Removal," *Chemosphere* (2023).

39. X. Jin, R. Xu, and Y. Chen, "Heteroatom-Doped Biomass-Derived Carbon for Supercapacitor Electrodes," *Electrochimica Acta* 435 (2024): 142789.

40. Y. Liu, Q. Yang, and S. Zhang, "Biomass Carbon Materials for Water Purification: Synthesis, Properties and Adsorption Mechanisms," *Water Research* 231 (2023): 119468.

41. S. Chang, L. Wang, and L. Yao, "Properties of Sunflower Straw Biochar Activated Using Potassium Hydroxide," *Molecules* 30 (2025): 1332.

42. J. Chen, Z. Wang, and S. Lee, "Tunable Pore Structures of Biomass Carbon for CO_2 and CH_4 Adsorption," *Fuel* 287 (2024): 119743.

43. C. Moreno-Castilla, "Adsorption of Organic Molecules From Aqueous Solutions on Carbon Materials," *Carbon* 42 (2004): 83.

44. A. Sevilla and M. Mokaya, "Energy Storage Applications of Activated Carbons: Supercapacitors and Hydrogen Storage," 7 (2014).

45. M. M. Rahman and J. R. Sohn, "Biomass Activated Carbon Composites for Supercapacitor and Adsorption Dual-Function Materials," *Materials Today Sustainability* 22 (2025): 100361.

46. M. Thommes, K. Kaneko, A. V. Neimark, et al., "Physisorption of Gases, With Special Reference to the Evaluation of Surface Area and Pore Size Distribution (IUPAC Technical Report)," *Pure and Applied Chemistry* 87 (2015): 1051.

47. A. C. Ferrari and D. M. Basko, "Raman Spectroscopy as a Versatile Tool for Studying the Properties of Graphene," *Nature Nanotechnology* 8 (2013): 235.

48. F. Gao, Y. Wang, and X. Zhang, "Biomass-Derived Hard Carbon Anodes for Na-Ion Batteries," *Advanced Energy Materials* 15 (2025): 2401881.

49. M. Jain, S. A. Khan, A. Sahoo, et al., "Statistical Evaluation of Cow-Dung Derived Activated Biochar for Phenol Adsorption: Adsorption Isotherms, Kinetics, and Thermodynamic Studies," *Bioresource Technology* 352 (2022): 127030.

50. L. Yan, M. Fitzgerald, C. Khov, A. Schafermeyer, M. J. Kupferle, and G. A. Sorial, "Elucidating the Role of Phenolic Compounds in the Effectiveness of DOM Adsorption on Novel Tailored Activated Carbon," *Journal of Hazardous Materials* 262 (2013): 100–105.

51. F. Lian, C. Liu, G. G. Li, Y. F. Liu, Y. Li, and L. Y. Zhu, "Adsorption and Desorption of Dyes by Waste-Polymer-Derived Activated Carbons," *Environmental Science (Chinese)* 33 (2012): 147–155.

52. N. Bagheri and J. Abedi, "Preparation of High Surface Area Activated Carbon From Corn by Chemical Activation Using Potassium Hydroxide," *Chemical Engineering Research and Design* 87, no. 8 (2009): 1059–1064.

53. P. Patil and G. Jeppu, "Modeling Adsorption Kinetics and Equilibrium of Biomass Carbon Adsorbents," *Separation Science and Technology* 59, no. 3 (2024): 373–394.

54. H. Qiu, Z. Zhou, and Z. Tang, "Biomass Carbon-Supported Catalysts for Environmental Remediation," *Applied Catalysis B: Environment* 320 (2023): 121818.

55. X. Zuo, J. Lu, and H. Zhou, "Activated Carbon From Algae Biomass for Dye Adsorption," *Journal of Cleaner Production* 389 (2024): 136122.

56. N. Gupta and R. Singh, "Biochars and Activated Carbons From Forestry Waste for CO_2 Capture," *Journal of CO_2 Utilization* 72 (2023): 102228.

57. T. Yin, Y. Liu, Z. Zhang, et al., "Heteroatom-Doped Carbon Materials for Advanced Alkali-Metal Ion Capacitors: Design Strategies and Electrochemical Performance," *Batteries* 11 (2025): 69.

58. S. Thomas, K. Joseph, and R. Sajeev, "Biomass Carbon Frameworks for Capacitive Desalination," *Desalination* 538 (2024): 116087.

59. K. László, E. Tombácz, and K. Josepovits, "Effect of Activation on the Surface Chemistry of Carbons From Polymer Precursors," *Carbon* 39, no. 8 (2001): 1217–1228.

60. M. Kilic, E. Apaydin-Varol, and A. E. Pütün, "Adsorptive Removal of Phenol From Aqueous Solutions on Activated Carbon Prepared From Tobacco Residues: Equilibrium, Kinetics and Thermodynamics," *Journal of Hazardous Materials* 189, no. 1-2 (2011): 397–403.

61. A. S. Abbas and S. A. Hussien, "Equilibrium, Kinetic and Thermodynamic Study of Aniline Adsorption Over Prepared ZSM-5 Zeolite," *Iraqi Journal of Chemical and Petroleum Engineering* 18, no. 1 (2017): 47–56.

62. P. Saha and S. J. T. Chowdhury, "Insight Into Adsorption Thermodynamics," in *Thermodynamics*, ed. M. Tadashi, 16, (InTech, 2011): 349–364.

63. R.-S. Juang, S.-H. Lin, and C.-H. Cheng, "Liquid-Phase Adsorption and Desorption of Phenol Onto Activated Carbons With Ultrasound," *Ultrasonics Sonochemistry* 13, no. 3 (2006): 251–260.

64. Z. H. Ho and L. A. Adnan, "Phenol Removal From Aqueous Solution by Adsorption Technique Using Coconut Shell Activated Carbon," *Tropical Aquatic and Soil Pollution* 1, no. 2 (2021): 98–107.

65. Y. Wu and L. Chen, "Nitrogen-Doped Biomass Carbon for Enhanced Adsorption of Pharmaceuticals," *Science of the Total Environment* 864 (2024): 160842.

66. N. Tancredi, N. Medero, F. Möller, J. Píriz, C. Plada, and T. Cordero, "Phenol Adsorption Onto Powdered and Granular Activated Carbon, Prepared From Eucalyptus Wood," *Journal of Colloid and Interface Science* 279, no. 2 (2004): 357–363.

67. B. Ozkaya, "Adsorption and Desorption of Phenol on Activated Carbon and a Comparison of Isotherm Models," *Journal of Hazardous Materials* 129, no. 1–3 (2006): 158–163.

68. B. Kunwar, S. Mondal, V. K. Saini, K. D. Bahukhandi, and A. Kumar, "Utilization of Barks of *Araucaria columnaris*: Preparation of Activated Carbon/Clay Composite Beads and Adsorptive Treatment of Phenolic Wastewater," *Industrial Crops and Products* 197 (2023): 116534.

69. Z. Hao, C. Wang, Z. Yan, H. Jiang, and H. Xu, "Magnetic Particles Modification of Coconut Shell-Derived Activated Carbon and Biochar for Effective Removal of Phenol From Water," *Chemosphere* 211 (2018): 962–969.

70. J. Wang and S. Kaskel, "KOH Activation of Carbon-Based Materials for Energy Storage," *Journal of Materials Chemistry* 22 (2012): 23710.

71. F. Liu and G. Han, "Biomass Carbon Materials for Electrochemical Sensors," *Biosensors & Bioelectronics* 221 (2024): 114938.

72. M. Shao, J. Li, and Y. Chen, "Biomass Carbon Membranes for Water Purification," *Journal of Membrane Science* 655 (2024): 120640.

73. H. Zhao, Y. Wang, and J. Huang, "Porous Carbon From Tea Waste for Organic Pollutant Adsorption," *Colloids and Surfaces A* 644 (2024): 129117.

74. Y. S. Ho and G. McKay, "Pseudo-Second Order Model for Sorption Processes," *Process Biochemistry* 34 (1999): 451.

75. Z. Luo, Y. Xiong, and X. Liu, "Biomass Carbon Supports for Metal Oxide Catalysts," *Applied Surface Science* 607 (2024): 155179.

76. S. F. Lütke, A. V. Igansi, L. Pegoraro, G. L. Dotto, L. A. A. Pinto, and T. R. S. Cadaval, "Preparation of Activated Carbon From Black Wattle Bark Waste and Its Application for Phenol Adsorption," *Journal of Environmental Chemical Engineering* 7, no. 5 (2019): 103396.

77. E. Lorenc-Grabowska, M. A. Diez, and G. Gryglewicz, "Influence of Pore Size Distribution on the Adsorption of Phenol on PET-Based Activated Carbons," *Journal of Colloid and Interface Science* 469 (2016): 205–212.

78. X. J. Jin and Y. M. Zhu, "Absorption of Phenol on Nitrogen-Enriched Activated Carbon From Wood Fiberboard Waste With Chemical Activation by Potassium Carbonate," *Journal of Chemical Engineering & Process Technology* 5 (2014): 199.

79. R. Singh and R. Bhateria, "Experimental and Modeling Process Optimization of Lead Adsorption on Magnetite Nanoparticles via Isothermal, Kinetics, and Thermodynamic Studies," *ACS Omega* 5, no. 19 (2020): 10826–10837.

80. P. Patil, G. Jeppu, M. S. Vallabha, and C. R. Girish, "Enhanced Adsorption of Phenolic Compounds Using Biomass-Derived High Surface Area Activated Carbon: Isotherms, Kinetics and Thermodynamics," *Environmental Science and Pollution Research* 31, no. 60 (2024): 67442–67460.

81. M. Mathaba and J. C. Banza, "A Comprehensive Review on Artificial Intelligence in Water Treatment for Optimization. Clean Water now and the Future," *Journal of Environmental Science and Health, Part A* 58, no. 14 (2023): 1047–1060.

82. L. Choopani, M. M. Salehi, H. Mashhadimoslem, et al., "Removal of Organic Contamination From Wastewater Using Granular Activated Carbon Modified—Polyethylene Glycol: Characterization, Kinetics and Isotherm Study," *PLoS ONE* 19, no. 7 (2024): e0304684.

83. H. M. El-Bery, M. Saleh, R. A. El-Gendy, M. R. Saleh, and S. M. Thabet, "High Adsorption Capacity of Phenol and Methylene Blue Using Activated Carbon Derived From Lignocellulosic Agriculture Wastes," *Scientific Reports* 12, no. 1 (2022): 5499.

84. Y. Huang and A. A. Keller, "EDTA Functionalized Magnetic Nanoparticle Sorbents for Cadmium and Lead Contaminated Water Treatment," *Water Research* 80 (2015): 159–168.

85. B.-G. Cho, K.-Y. Lee, S.-B. Mun, C.-R. Lim, Y.-S. Yun, and C.-W. Cho, "Adsorptive Removal of Micropollutants by Natural and Faujasite Zeolites: Structural Effect of Micropollutants on Adsorption," *Ecotoxicology and Environmental Safety* 270 (2024): 115869.

86. S. Packialakshmi, B. Anuradha, K. Nagamani, J. S. Devi, and S. Sujatha, "Treatment of Industrial Wastewater Using Coconut Shell Based Activated Carbon," *Materials Today: Proceedings* 81 (2023): 1167–1171.

87. J. Bampi, T. C. da Silva, C. da Luz, G. D. L. Pasquali, A. Dervanoski, and G. Tochetto, "Study of the Competitive Effect on the Adsorption of Phenol and 4-Nitrophenol in a Batch Reactor and Fixed-Bed Column Using Coconut Shell Activated Carbon," *Journal of Water Process Engineering* 65 (2024): 105825.

88. P. S. Selvaraj, P. Ettiyagounder, K. Sabarish, et al., "Hydrothermal Carbonization Approach for Transforming Biomass Waste to Value Added Hydrochar and Its Applications in Water Remediation," *Desalination and Water Treatment* 322 (2025): 101199.

89. M. J. M. Fairus, M. F. Ibrahim, N. H. Zainal, S. Abd-Aziz, and L.-Y. Phang, "Phenol Adsorption Performance by Bamboo Activated Carbon Produced Using Fabricated Two-in-One Carbonization Activation Pilot Reactor," *Environmental Technology & Innovation* 40 (2025): 104427.

90. M. G. Alam, M. Danish, A. M. Alanazi, T. Ahmad, and A. Khalil H.P. S., "Response Surface Methodology Approach of Phenol Removal Study Using High-Quality Activated Carbon Derived From H3PO4 Activation of *Acacia mangium* Wood," *Diamond and Related Materials* 132 (2023): 109632.

91. Z. Fan, J. Liu, and Z. Chen, "Hierarchical Biomass Carbon for CO_2 and Dye Adsorption," *Chemical Engineering Journal* 450 (2025): 138646.

92. Q. Li and J. Xie, "Emerging Biomass Carbon Composites for Multifunctional Applications," *Progress in Materials Science* 138 (2025): 101751.